arXiv:1601.07917v1 [q-bio.TO] 15 Dec 2015

Vortex dynamics in an idealized embryonic ventricle with trabeculae

Nicholas A. Battista[a,f,*], Andrea N. Lane[a,b], Leigh Ann Samsa[c,d], Jiandong Liu[d,e], Laura A. Miller[a,f]

[a]*Department of Mathematics, CB 3250, University of North Carolina, Chapel Hill, NC, 27599*
[b]*Department of Biostatistics, UNC Gillings School of Global Public Health, Chapel Hill, NC, 27599*
[c]*Department of Cell Biology and Physiology, University of North Carolina, Chapel Hill, NC 27599.*
[d]*McAllister Heart Institute, UNC School of Medicine, University of North Carolina, Chapel Hill, NC 27599*
[e]*Department of Pathology and Laboratory Medicine, University of North Carolina, Chapel Hill, NC 27599*
[f]*Department of Biology, 3280, University of North Carolina, Chapel Hill, NC, 27599*

Abstract

In vivo experiments have highlighted the importance of understanding hemodynamic forces, i.e., shear stress and pressure, in vertebrate cardiogenesis. In particular, the formation of the cardiac trabeculae is governed by a delicate interaction between hemodynamic forces, myocardial activity, and epigenetic signaling mechanisms, which are coupled with genetic regulatory networks. The fluid dynamics at the stage of development in which the trabeculae form is particularly complex, given the balance between inertial and viscous forces. Vortices, which cause changes in the magnitude and direction of flow, are sensitive to small perturbations in scale, morphology, and unsteadiness of the flow. The immersed boundary method was used to solve the fluid-structure interaction problem of fluid flow moving through an idealized chamber with trabeculae. Trabeculae heights were varied, and simulations were conducted for Reynolds numbers (Re) ranging from 0.01 to 100. Using either steady or pulsatile parabolic inflow conditions, both intracardial and intertrabecular vortices formed for biologically relevant parameter values. The bifurcation from smooth streaming flow to vortical flow depends upon the pulsation frequency, trabeculae geometry, and Re. Vorticity can be important in inducing shear stress at the endothelial layer and mixing within the developing chambers, which is believed to aid in chamber morphogenesis, valvulogenesis, and the formation of the trabeculae themselves.

Keywords: immersed boundary method, heart development, trabeculae, fluid dynamics, cavity flow

[☆]This is only an example

[*]I am corresponding author

Email addresses: nick.battista@unc.edu (Nicholas A. Battista), anlane@live.unc.edu (Andrea N. Lane), lam9@unc.edu (Laura A. Miller)

URL: battista.web.unc.edu (Nicholas A. Battista)

1. Introduction

Hemodynamic forces help regulate and drive organogenesis in developing embryos [24]. Forces such as shear stress and pressure may be key components that activate developmental regulatory networks [32]. These mechanical forces act on the cardiac cells, where the mechanical stimuli is then transmitted to the interior of the cell via intracellular signalling pathways, i.e., mechanotransduction. The notion that mechanical forces are essential for proper vertebrate cardiogenesis is not a recent idea. It was first investigated by Chapman in 1918 when chicken hearts were surgically dissected during embryogenesis, and their resulting circulatory system did not develop properly [6]. Moreover, the absence of erythrocytes when the embryonic heart begins beating and continues to grow supports the belief that the early developing heart does not pump for nutrient transport. This suggests that the function of the embryonic heart is to aid in its own growth as well as that of the circulatory system [5].

By obstructing flow in the venous inflow tract of developing hearts *in vivo*, experiments have illustrated the importance of regular hemodynamics in proper morphogenesis [15, 17, 36]. Gruber *et al.* [15] found that irregular blood flow can lead to hypoplastic left heart syndrome (HLHS), where the ventricle is too small or absent during the remainder of cardiogenesis. Hove *et al.* [17] observed that when inflow and outflow tracts are obstructed in 37 hpf zebrafish, peristaltic myocardial contractions continue to persist and neither valvulogenesis, cardiac looping, nor chamber ballooning occur. Similarly, de-Vos *et al.* [36] performed a similar experiment in HH-stage 17 chicken embryos whereby the venous inflow tract was obstructed temporarily. They noticed that all hemodynamic parameters decreased initially, i.e., heart rate, peak systolic velocity, time-averaged velocity, peak and mean volumetric flow, and stroke volume. However, only heart rate, time-averaged velocity, and mean volumetric flow recovered near baseline levels.

Trabeculae are particularly sensitive to changes in intracardiac hemodynamic shear stress [12]. Moreover, cardiac contraction is required for trabeculation to occur [28]. Trabeculae are bundles of muscle that protrude from the interior walls of the ventricles of the heart. The sensitivity of the trabeulae under varying mechanical loads is important when considering they may serve as important structures in which cellular mechanotransduction occurs, to help govern cardiogenetic processes. Trabeculation may also help regulate and distribute shear stress over the ventricular endocardium and enhance mixing. Furthermore, the presence of trabeculation may contribute to a more uniform transmural stress distribution over the cardiac wall [22]. Even subtle trabeculation defects spawning from slight modifications in hemodynamics may magnify over time. As the mechanical force distribution changes due to the absence of normal trabeculae, Neuregulin signalling, along with other genetic signals, are disrupted, leading to further deviations from healthy cardiogenesis. For example, zebrafish embryos that are deficient in the key Neuregulin co-receptor ErbB2 display severe cardiovascular defects including bradycardia, decreased fractional shortening, and impaired cardiac conduction [20]. Disrupted shear distributions in the ventricle leads to immature myocardial activation patterns, which perpetuate ventricular conduction and contractile deficiencies, i.e., arrhythmia, abnormal fractional shortening, and possibly ventricular fibrillation [27].

The fluid dynamics of heart development, particularly at the stage when the trabeculae form, is complex due to the balance of inertial and viscous forces. The Reynolds number, Re is a dimensionless number that describes the ratio of inertial to viscous forces in the fluid and is given as $Re = (\rho UL)/\mu$, where μ is the viscosity of the blood, ρ is the density of the blood, U is the characteristic velocity (often chosen as the average or peak flow rate), and L is the characteristic length (often chosen as the diameter of the chamber or vessel). During critical developmental stages such as cardiac looping and the formation of the trabeculae, $Re \approx 1$. In this regime, a number of fluid dynamic transitions can occur, such as the onset of vortical flow and changes in flow direction, that depend upon the morphology, size of the chambers, and effective viscosity of the blood. The flow is also unsteady, and the elastic walls of the heart undergo large deformations.

Since analytical solutions are not readily available, recent work has used computational fluid dynamics to resolve the flow in the embryonic heart. For example, DeGroff et al. [9] reconstructed the three-dimensional surface of a human heart embryo using a sequence of two-dimensional cross-sectional images at stages 10 and 11. The cardiac wall was fixed, and steady and pulsatile flows were driven through the chambers. They found streaming flows (particles released on one side of the lumen did not cross over or mix with particles released from the opposite side) without coherent vortex structures. Liu et al. [21] simulated flow through a three-dimensional model of a chick embryonic heart during stage HH21 (after about 3.5 days of incubation) at a maximum Re of about 6.9. They found that vortices formed during the ejection phase near the inner curvature of the outflow tract. More recently, Lee *et al.* [19] performed 2D simulations of the developing zebrafish heart with moving cardiac walls. They found unsteady vortices develop during atrial relaxation at 20-30 hpf and in both the atrium and ventricle at 110-120 hfp. Goenezen *et al.* [11] used subject-specific computational fluid dynamics (CFD) to model flow through a model of the chick embryonic heart outflow tract.

The numerical work described above, in addition to direct *in vivo* measurements of blood flow in the embryonic heart [17, 35], further supports that the presence of vortices is sensitive to changes in Re, morphology, and unsteadiness of the flow. Santhanakrishnan *et al.* [31] used a combination of CFD and flow visualization in dynamically scaled physical models to describe the fluid dynamic transitions that occur as the chambers balloon, the endocardial cushions grow, and the overall scale of the heart increases. They found that the formation of intracardial vortices depends upon the height of the endocardial cushions, the depth of the chambers, and the Re. Their paper only consider steady flows in an idealized two-dimensional chamber geometry with smooth, stationary walls.

In this paper, we expand upon the work of Santhanakrishnan *et al.* by considering both pulsatile flows and the addition of trabeculae in a 2D idealized ventricle. We use the immersed boundary method to solve the fluid structure interaction problem of flow through a rigid ventricular cavity. Because the goal of this paper is to map out the bifurcations in flow structure that occur as a result of unsteadiness of the flow, trabeculae height, and Re, we restrict the work to this idealized model of the ventricle. Even with these simplifications, we find a variety of interesting bifurcations in flow structures that occur over a biologically relevant morphospace.

Parameter	Value
a_V	1.0
b_V	0.8
w_{AV}	0.8
w_{SV}	0.8
r_T	0.10
$\frac{h_T}{b_V}$	$\{0, 0.02, 0.04, \ldots, 0.16\}$

Table 1: Table of geometric parameters used in the numerical model. The height of trabeculae, h_T, were varied for numerical experiments.

2. Methods

2.1. Model Geometry

A simplified two dimensional geometry of a 96 hpf zebrafish ventricle, which contains trabeculae, was constructed using Figure 1a. The ventricle was idealized as a half ellipse, with semi-major axis a_V and semi-minor axis b_V. It is tangentially laid within a channel, which emulates a cavity-flow geometry. The channel models the atrioventricular canal (AV canal), with width w_{AV}, which is modeled as equal to the sinus venosus (SV) width, w_{SV}. Six equally-spaced trabeculae were aligned within the ventricle. The model geometry is illustrated in Figure 1c.

The trabeculae geometry was modeled using the following perturbed Gaussian-like function,

$$T(x) = h_T \left(1 - \left(\frac{x}{r_T}\right)^2\right) e^{-\left(\frac{x}{0.7 r_T}\right)^8}, \tag{1}$$

where r_T and h_T are the radii and height of each trabecula, respectively. The full geometry can be seen in Figure(1). This geometry is used for both the physical and numerical models of the ventricle.

The geometric model parameters are found in Table(1), which were scaled from measurements from Figure(1a). The parameters describing the ventricle were held constant and are given as the chamber height, b_V, chamber width, a_V, and width of the AV canal and SV, w_{AV} and w_{SV} respectively. Note that the radii of the trabeculae, r_T, was also constant in all numerical simulations, while the height of the trabeculae, h_T, was varied.

2.2. Numerical Method

The immersed boundary method [26] was used to solve for the flow velocities within the geometric model from Section 2.1. The immersed boundary method has been successfully used to study the fluid dynamics of a variety of biological problems in the intermediate Reynolds number range, defined here as $0.01 < Re < 1000$ (see, for example, [18, 16, 4, 34]). The model consists of stiff boundaries that are immersed within an incompressible fluid

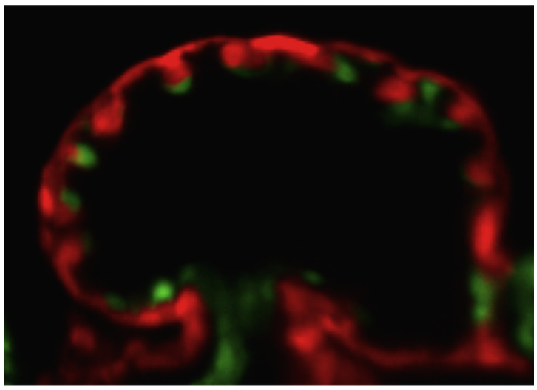

(a)

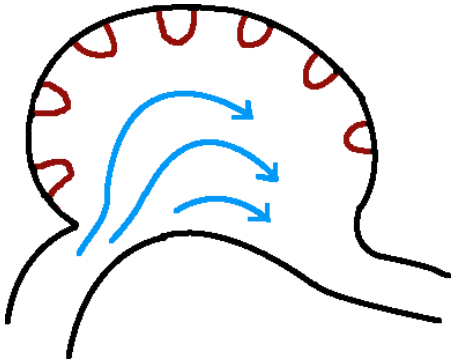

(b)

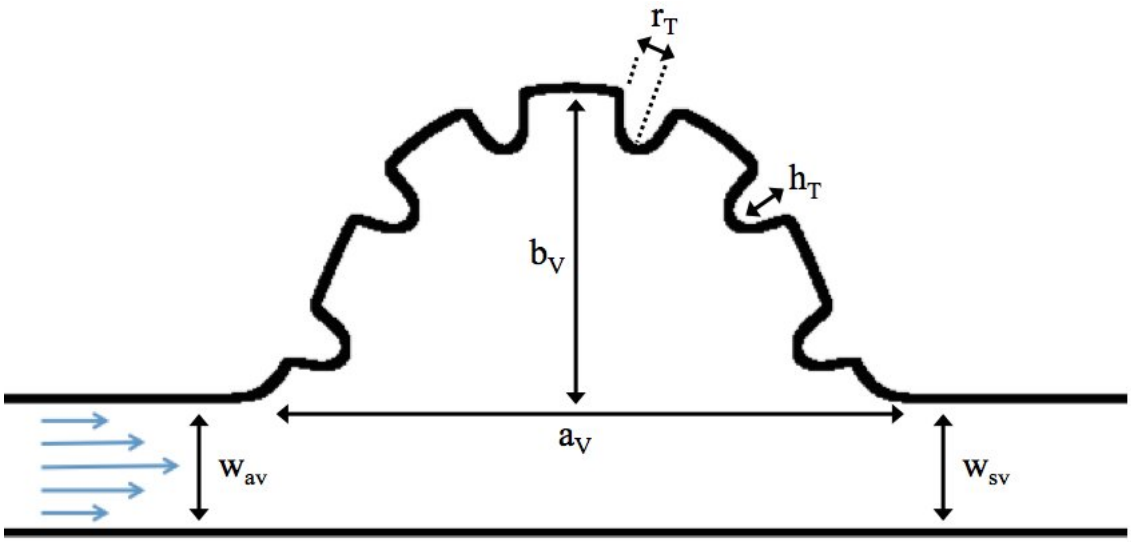

(c)

Figure 1: 1a is a snapshot of an embryonic zebrafish's ventricle at 96 hpf right using spinning disk confocal microscopy. The snapshot was taken right before its systolic phase. The protrusions into the ventriclular chamber are trabeculation. Image from Tg(cmlc2:dsRed)s879; Tg(flk1:mcherry)s843 embryos expressing fluorescent proteins that label the myocardium and endocardium, respectively [20]. Figure 1b illustrates the idea for our computational model geometry found in Figure 1c, that is, blood flows from the atrio-ventricular canal into the ventricle and then proceeds into the bulbus arteriosus. The computational model geometry is a flattened out rendition of 1b. The following geometric parameters, a_V and b_V, the semi-major and semi-minor axis of the elliptical chamber, h_T and r_T, the height and radii of the trabeculae, and w_{AV} and w_{SV}, the widths of the AV canal and sinus venosus respectively.

of dynamic viscosity, μ, and density, ρ. The fluid motion is described using the full 2D Navier-Stokes equations in Eulerian form, given a

$$\rho\left(\frac{\partial \mathbf{u}(\mathbf{x},t)}{\partial t}+\mathbf{u}(\mathbf{x},t)\cdot\nabla\mathbf{u}(\mathbf{x},t)\right)=-\nabla p(\mathbf{x},t)+\mu\Delta\mathbf{u}(\mathbf{x},t)+\mathbf{F}(\mathbf{x},t) \tag{2}$$

$$\nabla\cdot\mathbf{u}(\mathbf{x},t)=0, \tag{3}$$

where $\mathbf{u}(\mathbf{x},t)=(u(\mathbf{x},t),v(\mathbf{x},t))$ is the fluid velocity, $p(\mathbf{x},\mathbf{t})$ is the pressure, $\mathbf{F}(\mathbf{x},t)$ is the force per unit volume (area in $2D$) applied to the fluid by the immersed boundary, i.e., the ventricle geometry. The independent variables are the position, $\mathbf{x}=(x,y)$, and time, t. Eq.(2) is equivalent to the conservation of momentum for a fluid, while Eq.(3) is a condition mandating that the fluid is incompressible.

The interaction equations between the fluid and the immersed structure are given by

$$\mathbf{F}(\mathbf{x},t)=\int\mathbf{f}(r,t)\delta(\mathbf{x}-\mathbf{X}(r,t))dr \tag{4}$$

$$\mathbf{U}(\mathbf{X}(r,t),t)=\frac{\partial\mathbf{X}(r,t)}{\partial t}=\int\mathbf{u}(\mathbf{x},t)\delta(\mathbf{x}-\mathbf{X}(r,t))d\mathbf{x}, \tag{5}$$

where $\mathbf{X}(r,t)$ gives the Cartesian coordinates at time t of the material point labeled by Lagrangian parameter r, $\mathbf{f}(r,t)$ is the force per unit area imposed onto the fluid by elastic deformations in the boundary, as a function of the Lagrangian position, r, and time, t. Eq.(4) applies a force from the immersed boundary to the fluid grid through a delta-kernel integral transformation. Eq.(5) sets the velocity of the boundary equal to the local fluid velocity.

The force equations are specific to the application. In a simple case where a preferred motion or position is enforced, boundary points are tethered to target points via springs. The equation describing the force applied to the fluid by the boundary in Lagrangian coordinates is given by $\mathbf{f}(r,t)$ and is explicitly written as,

$$\mathbf{f}(r,t)=k_{target}\left(\mathbf{Y}(r,t)-\mathbf{X}(r,t)\right), \tag{6}$$

where k_{target} is the stiffness coefficient, and $\mathbf{Y}(\mathbf{r},\mathbf{t})$ is the prescribed Lagrangian position of the target structure. In all simulations the immersed structure was held nearly rigid by applying a force proportional to the distance between the location of the actual boundary and the preferred position. The deviation between the actual and preferred positions can be controlled with the variable k_{target}.

The fluid flow is driven through the immersed boundary using either pulsatile parabolic inflows or a linear ramp to steady parabolic inflow at the location of the AV canal. The equations describing the specific inflow boundary conditions are given in Table(**??**). A partial Neumann outflow condition is enforced in the direction of flow at the outlet. This outflow condition is given as

$$\begin{pmatrix}\frac{\partial u}{\partial\hat{n}}\\ v\end{pmatrix}=\begin{pmatrix}0\\0\end{pmatrix}. \tag{7}$$

Case	Inflow BC
Steady Inflow	$\mathbf{u_{in}} = \begin{pmatrix} \frac{V_{in}}{d_{AV}^2} \tanh(2t) \left(\frac{1}{4d_{AV}^2} - y^2 \right) \\ 0 \end{pmatrix}$
Pulsatile Inflow	$\mathbf{u_{in}} = \begin{pmatrix} \frac{V_{in}}{d_{AV}^2} \lvert \sin(2\pi f t) \rvert \left(\frac{1}{4d_{AV}^2} - y^2 \right) \\ 0 \end{pmatrix}$

Table 2: Inflow boundary conditions for both simulations, one pertaining to parabolic steady inflow and the other corresponding to a parabolic pulsatile inflow. The parameters used for the boundary conditions are f, the non-dimensional frequency, which is matched to the zebrafish heart at 96 hpf, and V_{in}, the maximum inflow velocity.

where u and v are the $x-$ and $y-$components of the fluid velocity, respectively, and $\frac{\partial u}{\partial n}$ is the directional derivative of the $x-$component of the velocity taken in the direction normal to the boundary of the fluid domain.

To determine the Re within the ventricle of a 4 dpf wild type zebrafish, the characteristic velocity, V_{zf} was taken as the average of the minimum and maximum velocity measured *in vivo*, and the characteristic length, L_{zf}, was taken along a diagonal within the ventricle from Figure(1a). The Re was then calculated as

$$Re = \frac{\rho_{zf} L_{zf} V_{zf}}{\mu_{zf}} = 1.07, \tag{8}$$

where $V_{zf} = 0.75\ cm/s$ [17], $\rho_{zf} = 1025\ kg/m^3$ [30], $\mu_{zf} = 0.0015\ kg/(ms)$ [23], and $L_{zf} = 208\ \mu m$. The characteristic frequency was chosen as $f = 3.95\ beats/s$ [22]. The dimensionless frequency may then be calculated as

$$\tilde{f} = \frac{L_{zf}}{V_{zf}} f_{zf} = 0.11. \tag{9}$$

For the mathematical model, the parameters values were chosen to keep the dimensionless frequency fixed at 0.10 for the pulsatile simulations. The Re was varied by changing the kinematic viscosity, $\nu = \mu/\rho$. The computational parameters are found in Table(2). For the simulations, the Re_{sim} is calculated using a characteristic length of w_{AV} and a characteristic velocity set to V_{in} (steady inflow) or $\frac{1}{2}V_{in}$ (pulsatile inflow). The simulations were performed for $Re_{sim} = 0.01, 0.05, 0.1, 0.5, 1, 5, 10, 20, 30, 40, 50, 100$. The stiffness of the target tethering points were chosen the minimize the deformations of the boundary, i.e, to keep it rigid, and was directly correlated to Re.

We used an adaptive and parallelized version of the immersed boundary method, IBAMR [13, 14]. IBAMR is a C++ framework that provides discretization and solver infrastructure for partial differential equations on block-structured locally refined Eulerian grids [3, 2] and on Lagrangian (structural) meshes. IBAMR also includes infrastructure for coupling Eulerian and Lagrangian representations.

The Eulerian grid on which the NavierStokes equations were solved was locally refined near the immersed boundaries and regions of vorticity with a threshold of $|\omega| > 0.05$. This

Cartesian grid was organized as a hierarchy of four nested grid levels, and the finest grid was assigned a spatial step size of $dx = D/1024$, where D is the length of the domain. The ratio of the spatial step size on each grid relative to the next coarsest grid was 1:4. The temporal resolution was varied to ensure stability. Each Lagrangian point of the immersed structure was chosen to be $\frac{D}{2048}$ apart (twice the resolution of the finest fluid grid).

T

3. Results

In this paper, we present the bulk flow structure over an idealized 2D model of a trabeculated ventricle for the cases of both steady and unsteady flow. The Re is varied from 0.01 to 100, and the trabecular heights are varied from zero to twice the biologically relevant case. Streamlines are used to show the direction of flow. The streamline graphs were generated using VisIt visualization software [8]. When interpreting streamlines, please note that a neutrally buoyant, small particle in the fluid will follow the streamline. The streamlines are drawn by making a contour map of the stream function, since the stream function is constant along the streamline. The stream function, $\psi(\mathbf{x}, t)$, in 2-D is defined by the following equations:

$$u(\mathbf{x}, t) = \frac{\partial \psi(\mathbf{x}, t)}{\partial y} \tag{10}$$

$$v(\mathbf{x}, t) = -\frac{\partial \psi(\mathbf{x}, t)}{\partial x} \tag{11}$$

The streamline colors correspond to smooth, streaming flow (blue) and vortical flow (orange).

3.1. Steady Flow through Trabeculated Chambers

Figure 2 shows the flow field streamlines for the case of steady flow through an idealized trabeculated embryonic ventricle. The numerical simulations span five orders of magnitude of Re, varying from 0.01 to 100, while trabeculae heights were set to $0 \leq \frac{h_T}{b_V} \leq 0.16$. Note that the biologically relevant case is $\frac{h_T}{b_V} = 0.08$

In the case of no trabeculae (left column), we find vortex formation only occurs for $Re \geq 15$, in agreement with the findings of [31]. For $Re \leq 10$, the flow bends around the cavity and no flow separation occurs. As Re is increased to 20, flow reversal occurs and a closed vortex is present along the left side of the cavity. The stagnation point is located between the orange and blue streamlines. To the left of this stagnation point, the flow moves along the endocardium from the right to left. To the right of the stagnation point, the flow moves right to left. As Re is further increased, the stagnation point moves to the right, and the intracardial vortex becomes larger until it becomes as large as the cavity itself for $Re = O(100)$.

When half-size biologically relevant trabeculae are introduced into the model ($\frac{h_T}{b_V} = 0.04$), similar flow fields emerge for the case of $Re \leq 10$. Although geometric perturbations now exist along the cavity lining, no flow separation occurs, whether intracardially or intertrabecularly. For $Re = 20$ we see a similar intracardial vortex to the case without trabeculae;

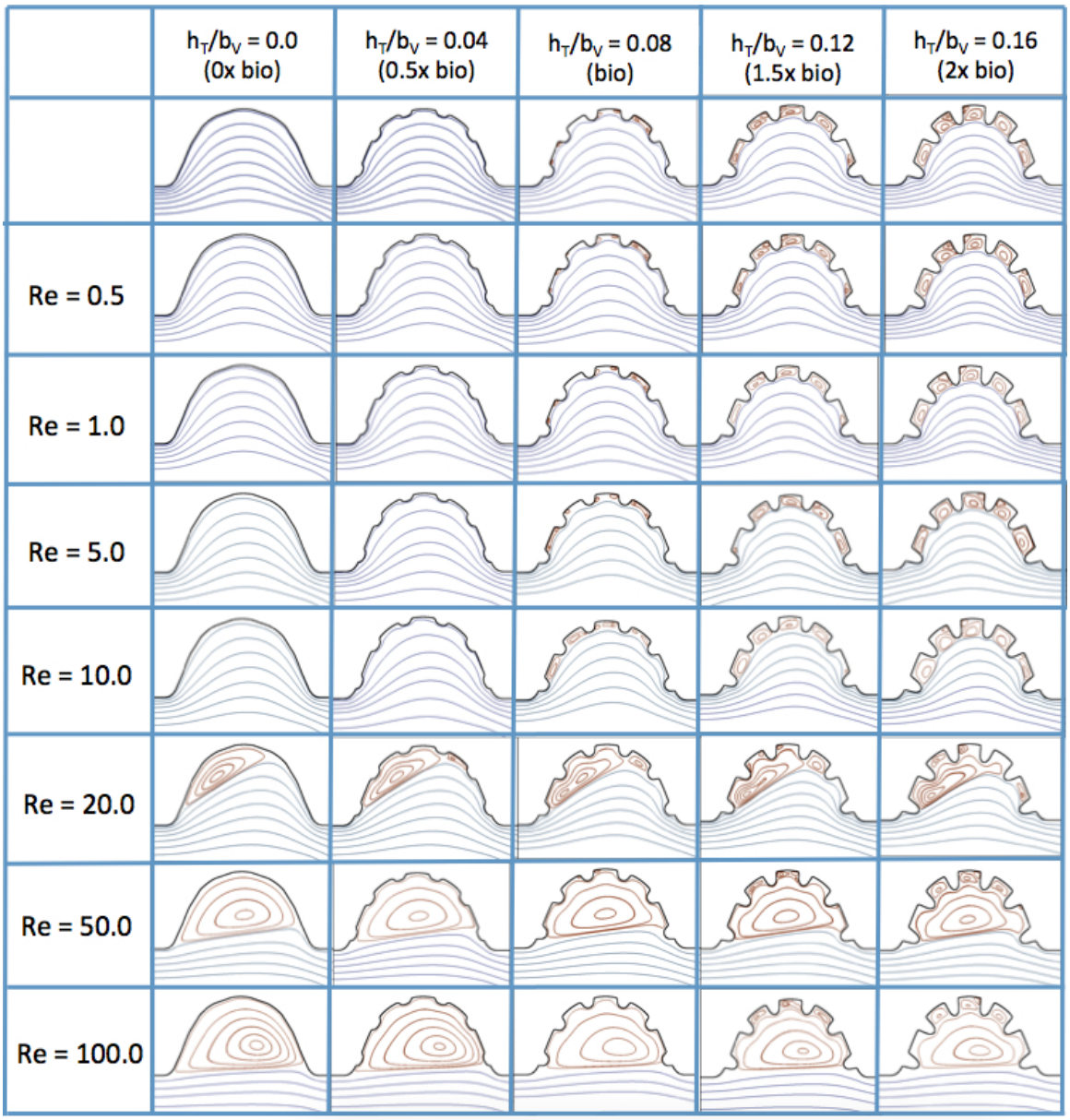

Figure 2: Streamline analysis performed for the case of steady flow into the trabeculated ventricle of a zebrafish at 96 hpf for varying Re and trabeculae heights.

however, it is also seen to weave along regions with trabeculae. Furthermore there is an emergence of an independent closed vortex along the right side between two trabeculae. For $Re \geq 50$, we find the presence of one large intracardial vortex wrapping around each trabeculae.

For biologically relevant trabeculae heights, there are closed intertrabecular vortices for Re as low as 0.01, while no intracardial vortices are present at these lower Re. Interestingly, not all intertrabecular regions have closed vortices. As Re is further increased from $Re = 5$ to $Re = 10$, the intertrabecular vortices grow in size. As in previous cases, a larger intracardial vortex forms at $Re = 20$. On the left hand side of the cavity, there is smooth flow from left to right around the trabeculae. On the right side of the cavity, independent closed vortices form between the trabeculae, and the flow is from right to left. For $Re \geq 50$, a large intracardial vortex forms and no intertrabecular vortices persist.

For trabeculae heights higher than the biologically relevant range, there exist intertrabecular vortices for Re as low as $Re = 0.01$; however, compared to the previous biologically relevant case, there are vortices between every adjacent pair of trabeculae. Moreover, because the trabeculae extend further into the ventricular cavity, these vortices are larger than in previous cases. Intracardial vortices do not develop until $Re \geq 20$, where there is the presence of one large intracardial vortex on the left side of the cavity. When $Re = 20$ and $\frac{h_T}{b_V} = 0.12$, the intracardial vortex only wraps itself around the first four trabeculae with flow moving from left to right. A single intertrabecular vortex forms in the fourth trabecular valley. When $Re = 20$ and $\frac{h_T}{b_V} = 0.16$, the intracardial vortex extends over the left five trabeculae, with an intertrabecular vortex only in last valley between trabeculae on the right side. For $Re \geq 50$, there is the formation of a large intracardial vortex extending throughout the cavity. However, both the trabeculae heights and Re are large enough that this vortex does not wrap around each trabeculae, and intertrabecular vortices are able to form.

3.2. Pulsatile Flow through Trabeculated Chambers

In the second set of simulations, the flow was pulsed through the idealized chambers at a dimensionless frequency close to that reported for a 96 hpf embryonic zebrafish ($\tilde{f} = 1.0$). The Re was set to 0.1, 1.0, 10 and 100. The dimensionless trabecular heights, $\frac{h_T}{b_V}$ were varied from 0.0 to 0.16. Recall that the biologically relevant Re is about one, and the biologically relevant dimensionless trabecular height is about 0.08. Snapshots of the streamlines showing the flow patterns are given for each simulation for either 9 or 10 time points during the pulse.

Figures 3 and 4 show streamline plots taken at 9 snapshots in time for lower Re cases, $Re = 0.1, 1.0$, respectively. The streamlines are shown for 5%, 10%, 20%, 40%, 50%, 80%, 90%, 95%, and 100% of the pulse. Finer increments in time are given towards the beginning and end of the pulse to illustrate the rapidly changing dynamics. The $Re = 0.1, 1.0$ cases show similar results. For the majority of the pulse, the flow moves smoothly from left to right within the ventricle. In between the trabeculae, vortices form during most of the pulse if the dimensionless trabecular height is at least 0.08. The development of these vortices causes the flow near the endothelial cells to move from right to left between the trabeculae and from left to right on the top of the trabeculae. In most cases, transient vortices form as

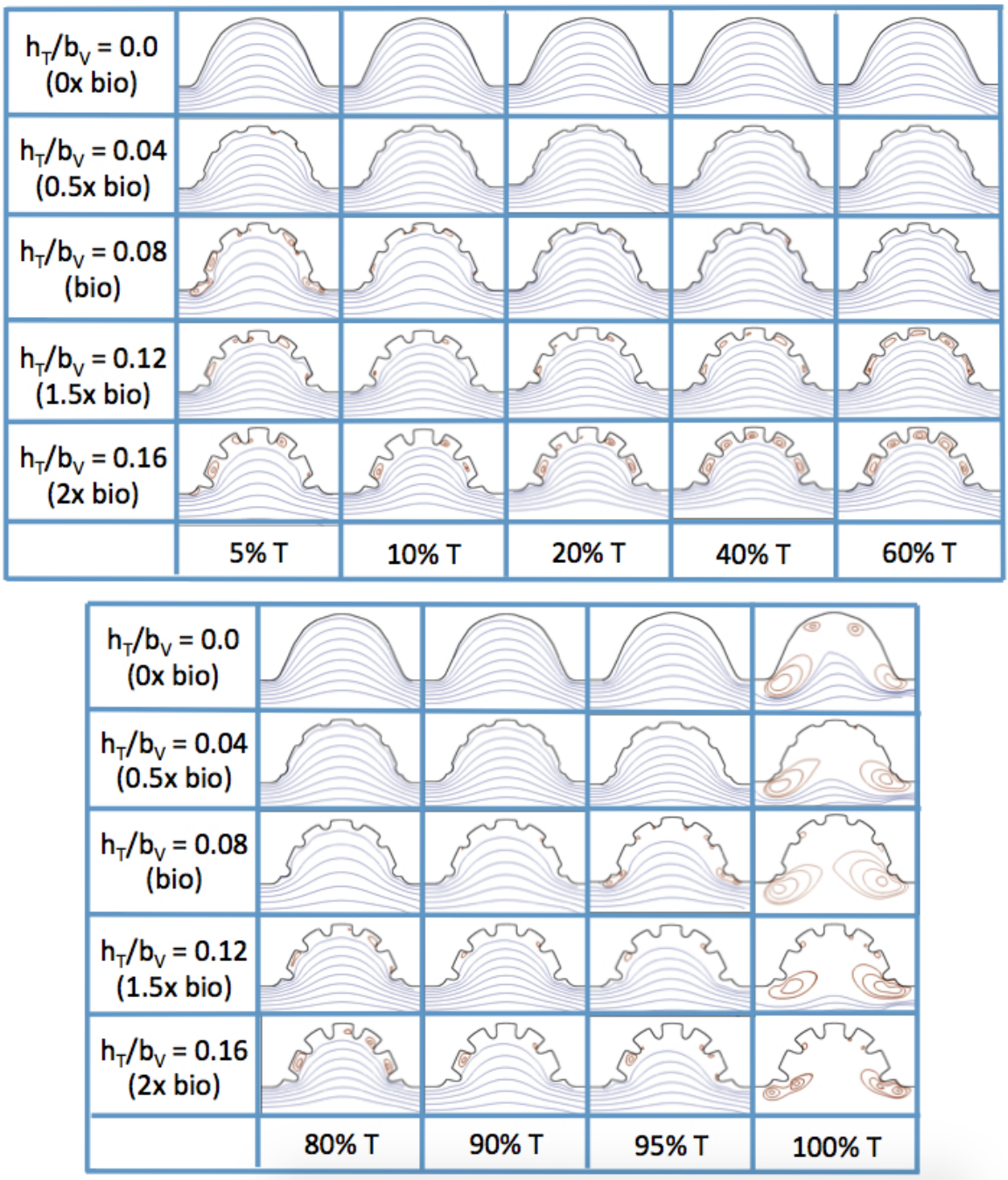

Figure 3: Streamline analysis performed for the case of pulsatile flow into the trabeculated ventricle of a zebrafish at 96 hpf for $Re = 0.1$ and varying trabeculae heights.

the flow is decelerated at the end of the pulse. For $Re = 1.0$, intertrabecular vortices form for small trabeculae, $\frac{h_T}{b_V} = 0.04$, as the flow decelerates.

Figure 5 shows streamline plots for $Re = 10$ at ten evenly spaced times during a pulse. Intertrabecular vortices form during the first half of the pulse if the dimensionless trabecular height is at least 0.04. For all geometries, intracardial vortices form during the last half of the pulse. The formation of the intracardial vortex annihilates the intertrabecular vortices, at least initially. The intracardial vortices form on the upstream side of the chamber, and grow to fill the entire chamber by the end of the pulse. The intertrabecular vortices form again towards the end of the pulse for $\frac{h_T}{b_V} = 0.12, 0.16$. Note that the presence of the intracardial vortex causes the intertrabecular vortices to change direction so that they spin clockwise (and the intracardial vortices spin counterclockwise).

The results of the inertial dominated case, $Re = 100$, are shown in Figure 6. In all cases, a large intracardial vortex that fills the entire chamber is observed at the end of the pulse and beginning of the next pulse. As the flow accelerates, the intracardial vortex is pushed downstream, and another intracardial vortex begins to form ($t = 0.4T - 0.5T$). One or more oppositely spinning vortices form between the trabeculae or between the two counterclockwise spinning intracardial vortices when $t = 0.5T$. The upstream intracardial vortex combines with the original intracardial vortex such that one large intracardial vortex is observed around $t = 0.7T$. When this occurs, the oppositely spinning vortices are annihilated. For $\frac{h_T}{b_V} \geq 0.08$, oppositely spinning intertrabecular vortices reappear at the end of the pulse.

4. Conclusions

Two-dimensional immersed boundary simulations were used to solve for the flow fields within an idealized model of a trabeculated ventricle of the zebrafish embryonic heart. Our results show that a large intracardial vortex forms around $Re \approx 20$ when steady flow is pushed through the chamber. When the flow is pulsatile, the intracardial vortex begins to form around $Re \approx 10$. In general, pulsatile flow lowers the Re and trabeculae height needed to generate vortices. For both steady and unsteady flows as the trabeculae grow into the chamber, another bifurcation occurs in which small vortices form between each trabecula. Depending upon the Re and the morphology, the intertrabecular vortices can form without the presence of a large intracardial vortex. In other cases, typically at higher Re, both the intracardial and intertrabecular vortices form. The presence of intracardial vortices changes the direction of the intertrabecular vortices.

This work focused specifically on the presence or absence of vortices given their significance to both the magnitude and direction of flow as well as the mixing patterns within the ventricle. When an intracardial vortex forms, the direction of the flow changes. When an intracardial vortex forms in unsteady flow, the direction of flow can change during the beat cycle, and the stagnation point moves along the cardiac wall. Since endothelial cells are known to sense and respond to changes in both magnitude and direction of flow, the formation and motion of these vortices could be an important epigenetic signal. The simulations revealed unexpected complexities in vortex dynamics as bulk flow moves from left to right through the chamber. When an intracardial vortex forms in absence of intertrabecular

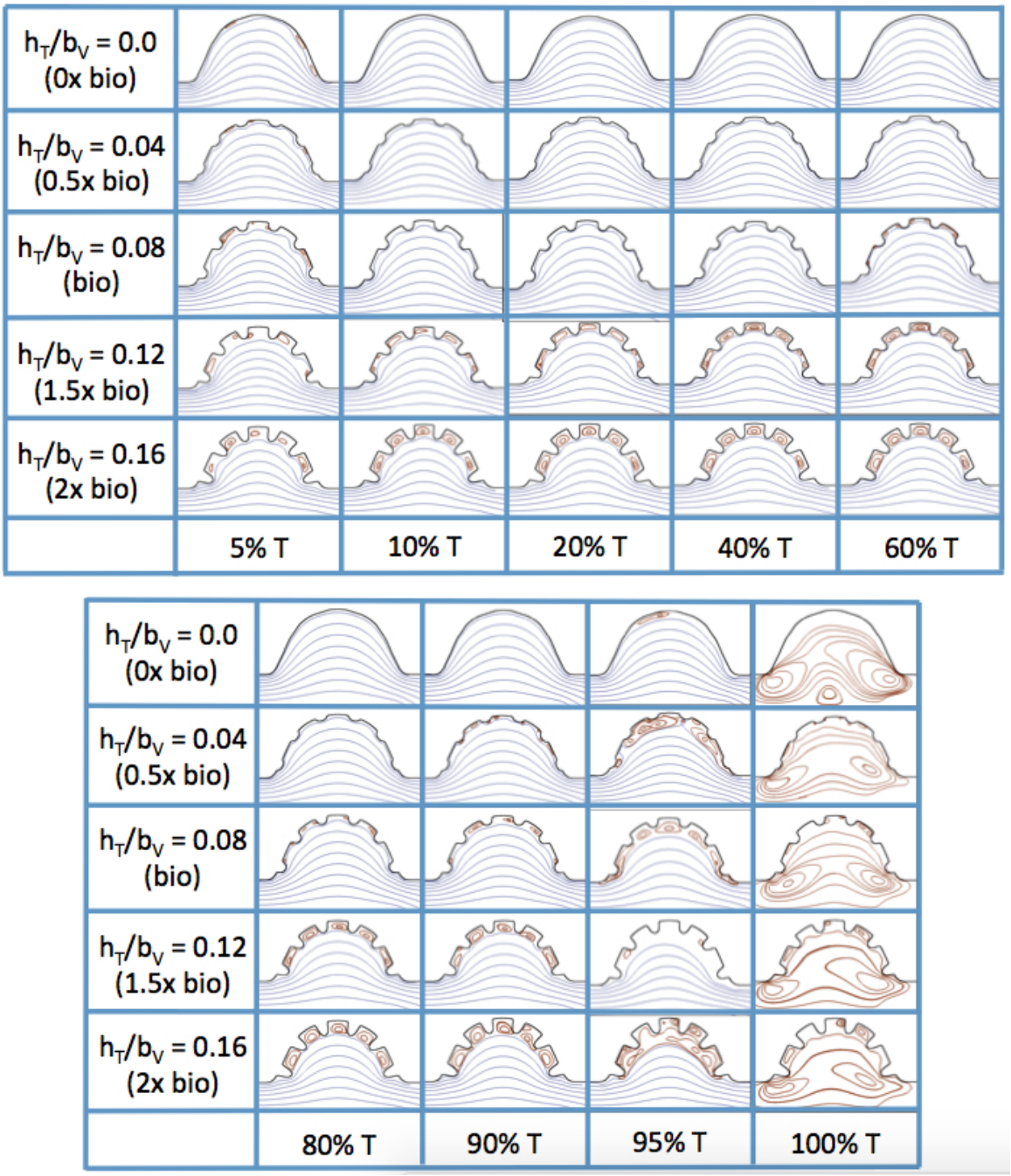

Figure 4: Streamline analysis performed for the case of pulsatile flow into the trabeculated ventricle of a zebrafish at 96 hpf for $Re = 1.0$ and varying trabeculae heights.

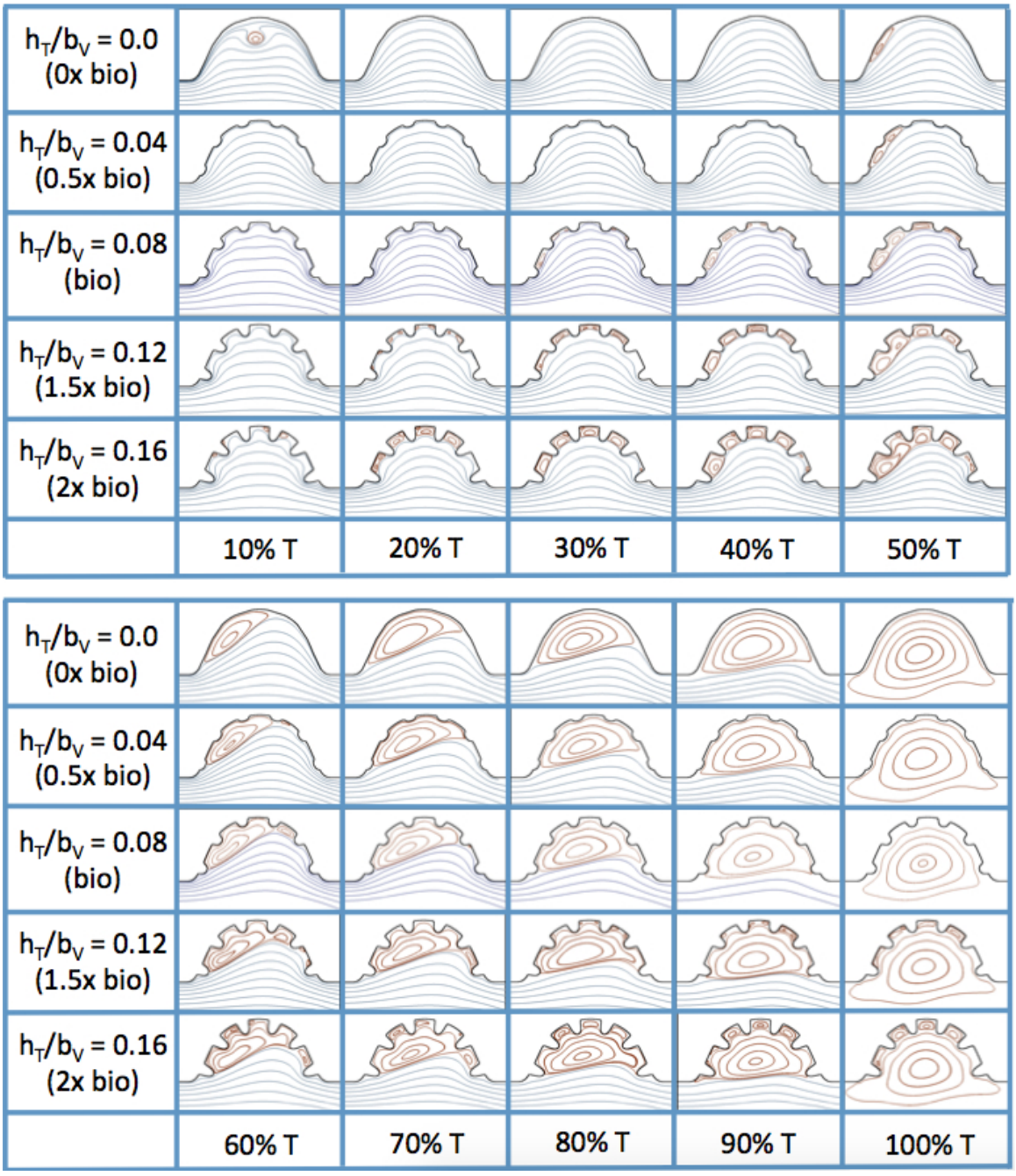

Figure 5: Streamline analysis performed for the case of pulsatile flow into the trabeculated ventricle of a zebrafish at 96 hpf for $Re = 10.0$ and varying trabeculae heights.

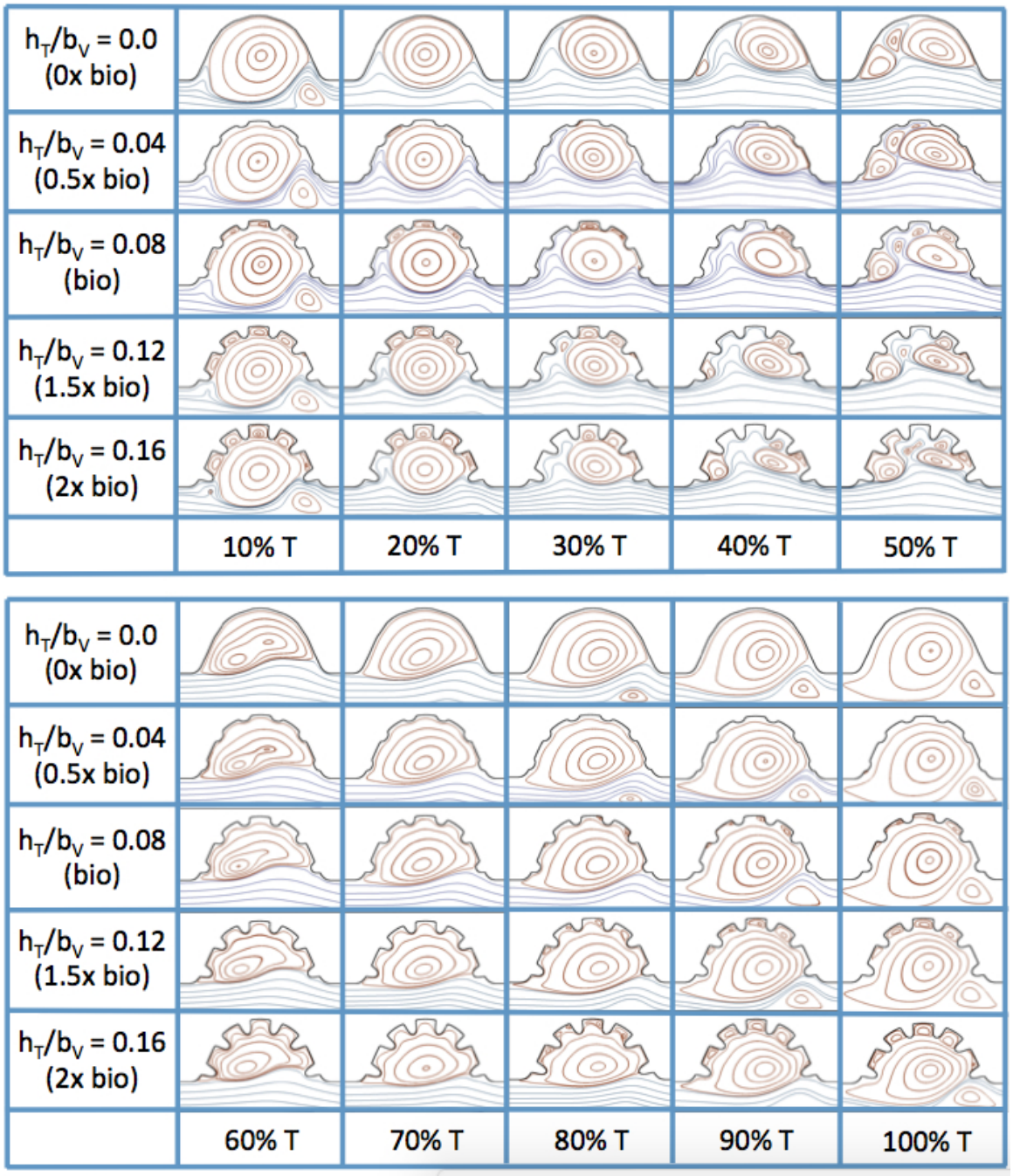

Figure 6: Streamline analysis performed for the case of pulsatile flow into the trabeculated ventricle of a zebrafish at 96 hpf for $Re = 100$ and varying trabeculae heights.

vortices, the flow at the endocardial wall moves from right to left. When the intertrabecular vortices form in absence of an intracardial vortex, the flow again moves from right to left. When both intertrabecular and intracardial vortices form, the flow moves from left to right since the intertrabecular and intracardial vortices spin in opposite directions. We also observe cases where not all intertrabecular spaces have a vortex. In such cases, the flow between different trabeculae will move in different directions.

Importantly, this idealized study demonstrates that small changes in viscosity, scale, morphology, and contraction dynamics can substantially influence bulk flow properties in the embryonic heart. This presents an interesting challenge since each of these parameters is continuously changing during growth. In addition, estimating the effective viscosity of the embryonic blood is nontrivial. Given the sensitivity of the flow to such small perturbations, it is necessary to use well resolved numerical grids that are experimentally validated.

Furthermore, it is evident that there is a strongly coupled relationship between intracardial hemodynamics, genetic regulatory networks, and cardiac conduction. Besides contractions of the myocardial cells, which in turn drive blood flow, hemodynamics are directly involved in proper pacemaker and cardiac conduction tissue formation [33]. Moreover, shear stress is found to govern the conduction velocity distribution of action potentials within the myocardium [27]. It is important to note that changes in the conduction properties of the embryonic heart will also affect the intracardial shear stresses, pressures and patterns of cyclic strains.

The cyclic stresses and strains of the cardiomyocytes can also help shape the overall architecture of the trabeculated ventricle. The dynamics of these strains depend upon the intracardial fluid dynamics. For example, greater resistant to flow will induce larger cyclic stresses and possibly reduced cyclic strains. It is known that cyclic strains initiate myogenesis in the cellular components of primitive trabeculae. [10] Since trabeculation first occurs near peak stress sites in the ventricle, altering blood flow may directly produce structural and morphological abnormalities in cardiogenesis. Previous work focusing on hemodynamic unloading in an embryonic heart has resulted in disorganized trabeculation and arrested growth of trabeculae [29, 25, 1]. On the other hand, embryos with a hypertrabeculated ventricle also experience impaired cardiac function. [25]

The exact mechanisms of mechanotransduction are not yet clearly understood [37]. Mechanically sensitive biochemical signals are thought to be propagated throughout a pipeline of epigenetic signaling mechanisms, which may lead to regulation of gene expression, cellular differentiation, proliferation, and migration [7]. *In vitro* studies have discovered that endothelial cells can detect shear stresses as low as 1 dyn/cm^2 [17] resulting in up or down regulation of gene expressions. Embryonic zebrafish hearts beyond 36 hpf are known to undergo shear stresses on the order of $\sim 8 - 15$ dyn/cm^2, and such magnitudes of shear stress can cause cytoskeletal rearrangement [17]. Mapping out the connection between fluid dynamics, the resulting forces, and the mechanical regulation of developmental regulatory networks will be critical for a global understanding of the process of heart development.

5. Acknowledgements

The authors would like to thank Steven Vogel for conversations on scaling in various hearts. We would also like to thank Lindsay Waldrop, Austin Baird, and William Kier for discussions on embryonic hearts. This project was funded by NSF DMS CAREER #1151478 awarded to L.A.M. Funding for N.A.B. and L.A.S. was provided from an National Institutes of Health T32 grant [HL069768-14; PI, Nobuyo Maeda].

References

[1] Bartman T, Walsh EC, Wen KK, McKane M, Ren J, Alexander J, Rubenstein PA, Stainier DY (2004) Early myocardial function affects endocardial cushion development in zebrafish. PLoS Biol 2:E129

[2] Berger MJ, Colella P (1989) Local adaptive mesh refinement for shock hydrodynamics. J Comput Phys 82(1):64–84

[3] Berger MJ, Oliger J (1984) Adaptive mesh refinement for hyperbolic partial-differential equations. J Comput Phys 53(3):484–512

[4] Bhalla A, Griffith B, Patankar N (2013) A forced damped oscillation framework for undulatory swimming provides new insights into how propulsion arises in active and passive swimming. PLOS Comput Biol 9:e1003,097

[5] Burggren W (2004) What is the purpose of the embryonic heart beat? or how facts can ultimately prevail over physiological dogma. Physiological and Biochemical Zoology 77:333345

[6] Chapman W (1918) The effect of the heart-beat upon the development of the vascular system in the chick. Am J Anat 23:175203

[7] Chen L, Wei S, Chiu J (2014) Mechanical regulation of epigenetics in vascular biology and pathobiology. J Cell Mol Med 11:437–448

[8] Childs H, Brugger E, Whitlock B, Meredith J, Ahern S, Pugmire D, Biagas K, Miller M, Harrison C, Weber GH, Krishnan H, Fogal T, Sanderson A, Garth C, Bethel EW, Camp D, Rübel O, Durant M, Favre JM, Navrátil P (2012) VisIt: An End-User Tool For Visualizing and Analyzing Very Large Data. In: High Performance Visualization–Enabling Extreme-Scale Scientific Insight, pp 357–372

[9] DeGroff CG, Thornburg BL, Pentecost JO, Thornburg KL, Gharib M, *et al* DJS (2003) Flow in the early embryonic human heart. Pediatric Cardiology 24:375380

[10] Garita B, Jenkins M, Han M, Zhou C, VanAuker M, Rollins A, Watanabe J, Fujimoto J, Linask K (2011) Blood flow dynamics of one cardiac cycle and relationship to mechanotransduction and trabeculation during heart looping. Am J Physiol Heart Circ Physiol 300:H879–H891

[11] Goenezen S, Chivukula VK, Midgett M, Phan L, Rugonyi S (2015) 4d subject-specific inverse modeling of the chick embryonic heart outflow tract hemodynamics. Biomech Model Mechanobiol

[12] Granados-Riveron J, Brook D (2012) The impact of mechanical forces in heart morphogenesis. Circ Cardiovasc Genet 5:132–142

[13] Griffith B (2014) An adaptive and distributed-memory parallel implementation of the immersed boundary (ib) method. URL `https://github.com/IBAMR/IBAMR`

[14] Griffith B, Hornung R, McQueen D, Peskin C (2007) An adaptive, formally second order accurate version of the immersed boundary method. J Comput Phys 223:1049

[15] Gruber J, Epstein J (2004) Development gone awry-congenital heart disease. Circulation Research 94:273–283

[16] Hershlag G, Miller LA (2011) Reynolds number limits for jet propulsion: a numerical study of simplified jellyfish. J Theor Biol 285:84–95

[17] Hove JR, Koster RW, Forouhar AS, Acevedo-Bolton G, Fraser SE, Gharib M (2003) Intracardiac fluid forces are an essential epigenetic factor for embryonic cardiogenesis. Nature 421(6919):172–177

[18] Jung E, Peskin C (2001) 2-d simulations of valveless pumping using immersed boundary methods. SIAM Journal on Scientific Computing 23:19–45

[19] Lee J, Moghadam ME, Kung E, Cao H, Beebe T, Miller Y, Roman BL, Lien CL, Chi NC, Marsden AL, Hsiai TK (????) Moving domain computational fluid dynamics to interface with an embryonic model of cardiac morphogenesis. PLoS One 8:e72,924

[20] Liu J, Bressan M, Hassel D, Huisken J, Staudt D, amd K Poss KK, Mikawa T, Stainier Y (2010) A dual role for erbb2 signaling in cardiac trabeculation. Development 137:3867–3875

[21] Liu RSPJTK A (2007) Finite element modeling of blood flow-induced mechanical forces in the outflow tract of chick embryonic hearts. Computers and Structures 85:727–738

[22] Malone M, Sciaky N, Stalheim L, Klaus H, Linney E, Johnson G (2007) Laser-scanning velocimetry: A confocal microscopy method for quantitative measurement of cardiovascular performance in zebrafish embryos and larvae. BMC Biotechnology 7:40

[23] Mohammed M, Roubaie S, Jahnsen E, Jones E (2011) Drawing first blood: Measuring avian embryonic blood viscosity. SURE Poster Presentation 61:33–45
[24] Patterson C (2005) Even flow: Shear cues vascular development. Arteriosclerosis, Thrombosis, and Vascular Biology 25:17611762
[25] Peshkovsky C, Totong R, Yelo D (2011) Dependence of cardiac trabeculation on neuregulin signaling and blood flow in zebrafish. Developmental Dynamics 240(2):446456
[26] Peskin C (2002) The immersed boundary method. Acta Numerica 11:479–517
[27] Reckova M, Rosengarten C, deAlmeida A, Stanley CP, Wessels A, Gourdie RG, Thompson RP, Sedmera D (2003) Hemodynamics is a key epigenetic factor in development of the cardiac conduction system. Circ Res 93:77
[28] Samsa LA, Givens C, Tzima E, Didier Y, Stainer R, Qian L, Liu J (????) Cardiac contraction activates endocardial notch signaling to modulate chamber maturation in zebrafish
[29] Sankova B, Machalek J, Sedmera D (2010) Effects of mechanical loading on early conduction system differentiation in the chick. Am J Physiol Heart Circ Physiol 298:1571–1576
[30] Santhanakrishnan A, Miller LA (2011) Fluid dynamics of heart development. Cell Biochem Biophys 61:1–22
[31] Santhanakrishnan A, Nhi N, Cox J, Miller LA (2009) Flow within models of the vertebrate embryonic heart. J Theor Biol 259:449–461
[32] Tarbell JM, Weinbaum S, Kamm RD (2005) Cellular fluid mechanics and mechanotransduction. Ann Biomed Eng 33:1719–1723
[33] Tucker DC, Snider C, Jr WTW (1988) Pacemaker development in embryonic rat heart cultured *in oculo*. Pediatric Research 23:637–642
[34] Tytell E, Hsu C, Williams T, A Cohen LF (2010) Interactions between internal forces, body stiffness, and fluid environment in a neuromechanical model of lamprey swimming. Proc Natl Acad Sci 107:19,83219,837
[35] Vennemann P, Kiger KT, Lindken R, Groenendijk BCW, de Vos SS, ten Hagen *et al* TLM (2006) In vivo micro particle image velocimetry measurements of blood-plasma in the embryonic avian heart. Journal of Biomechanics 39:11911200
[36] Vos SSD, Ursem N, Hop W, Wladimirioff J, Groot AGD, Poelmann R (2003) Acutely altered hemodynamics following venous obstruction in the early chick embryo. J Exp Biol 206:1051–1057
[37] Weinbaum S, Zhang X, Han Y, Vink H, Cowin S (2003) Mechanotransduction and flow across the endothelial glycoalyx. PNAS 100:7988–7995